A GaAs-based self-aligned stripe distributed feedback laser

2016 Semicond. Sci. Technol. 31 085001

(http://iopscience.iop.org/0268-1242/31/8/085001)

OPEN ACCESS
IOP Publishing
Semiconductor Science and Technology
Semicond. Sci. Technol. **31** (2016) 085001 (6pp)
doi:10.1088/0268-1242/31/8/085001

A GaAs-based self-aligned stripe distributed feedback laser

H Lei[1], B J Stevens[2], P W Fry[2], N Babazadeh[1], G Ternent[3], D T Childs[3] and K M Groom[1]

[1] Department of Electronic & Electrical Engineering, The University of Sheffield, Nanoscience & Technology Building, North Campus, Broad Lane, Sheffield, S3 7HQ, UK
[2] EPSRC National Centre for III-V Technologies, Department of Electronic & Electrical Engineering, The University of Sheffield, Nanoscience & Technology Building, North Campus, Broad Lane, Sheffield, S3 7HQ, UK
[3] School of Engineering, University of Glasgow, Glasgow, G12 8LT, Scotland, UK

E-mail: k.m.groom@sheffield.ac.uk

Received 23 March 2016, revised 12 May 2016
Accepted for publication 26 May 2016
Published 23 June 2016

Abstract

We demonstrate operation of a GaAs-based self-aligned stripe (SAS) distributed feedback (DFB) laser. In this structure, a first order GaInP/GaAs index-coupled DFB grating is built within the p-doped AlGaAs layer between the active region and the n-doped GaInP opto-electronic confinement layer of a SAS laser structure. In this process no Al-containing layers are exposed to atmosphere prior to overgrowth. The use of AlGaAs cladding affords the luxury of full flexibility in upper cladding design, which proved necessary due to limitations imposed by the grating infill and overgrowth with the GaInP current block layer. Resultant devices exhibit single-mode lasing with high side-mode-suppression of >40 dB over the temperature range 20 °C–70 °C. The experimentally determined optical profile and grating confinement correlate well with those simulated using Fimmwave.

Keywords: self-aligned stripe laser, distributed feedback laser, GaAs

(Some figures may appear in colour only in the online journal)

GaAs-based distributed feedback (DFB) lasers provide a robust, portable and low cost solution to enable a broad range of applications in spectroscopy, gas sensing, THz generation, and display. DFB lasers are typically available on GaAs as ridge lasers, with either laterally loss-coupled gratings [1] and more recently using buried index-coupled grating approaches incorporating combinations of GaAs, AlGaAs and InGaP [2, 3]. Buried heterostructures allow small lateral sizes, low threshold currents, good thermal management, and excellent fundamental mode stability compared with ridge waveguides, which can also suffer surface recombination, carrier spreading and poor fibre coupling efficiencies. They are typically used in directly modulated InP telecoms lasers. As with DFB lasers, buried heterostructures are commonplace on InP, where DFB gratings are incorporated within the buried heterostructure laser to realise rapidly modulated telecoms lasers. However, they are not commonly available on GaAs and approaches to their realisation include regrowth over potentially oxidised aluminium-containing layers, etch/regrowth in the same reactor [4], or use of InGaP cladding [5]. We have previously reported use of a GaAs/InGaP regrowth process to enable self-aligned stripe (SAS) lasers to be manufactured on GaAs [6]. In our GaAs-based SAS process, no aluminium is exposed to atmosphere prior to regrowth. Furthermore, since $Al_xGa_{1-x}As$ is lattice matched to GaAs for all compositions of x, this permits a significant amount of flexibility in waveguide design, and provides attractive benefits for future GaAs based photonic integrated circuits.

Our previous DFB [2] and SAS [6] laser reports describe structures realised with a single overgrowth and not specifically designed to be integrated together. In this paper, we

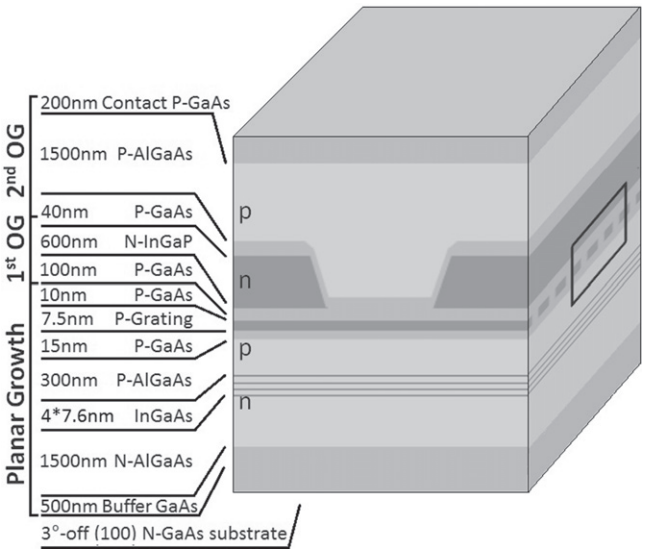

Figure 1. Schematic diagram of the layer structure that defines the self-aligned stripe DFB laser.

demonstrate the realisation of a SAS–DFB laser emitting ~1000 nm, based on a three-stage growth process (i.e. 2 overgrowths). Following resolution of the competing requirements of epitaxial planarisation and optical confinement, basic device characteristics are demonstrated. We discuss the design considerations governing operation of the laser, imposed by limitations to the regrowth process.

Planar growth and first overgrowth

A schematic diagram of our SAS–DFB laser is shown in figure 1, together with figure 2(a) showing a transmission electron micrograph (TEM) taken along a cross-section running parallel to the stripe. Figure 2(b) shows the guided mode profile simulated using Fimmwave software, by Photon Design. An n-doped $Al_{0.42}Ga_{0.58}As$ lower cladding layer was grown using metal-organic vapour phase epitaxy above a 500 nm GaAs buffer layer on an n-doped GaAs substrate which was mis-oriented by 3° to the (110) direction.

Above this, partially strain-balanced quantum wells (QWs) emitting ~990 nm were grown within a waveguide structure comprising 4 × 7.6 nm $In_{0.17}Ga_{0.83}As$ QWs separated by 10 nm $Ga_{0.9}AsP_{0.1}$ strain balancing layers. 50 nm GaAs was grown on either side to complete the waveguide core. 300 nm p-doped $Al_{0.42}Ga_{0.58}As$ was grown above the core prior to growth of the grating layer. The first order DFB grating layer comprised a 7.5 nm thick GaInP layer (lattice matched to GaAs) sandwiched between 15 and 10 nm thick GaAs layers. Following patterning by electron beam lithography, gratings were formed by first dry etching through the GaAs top layer using an argon reactive ion etch process, before wet etching through the GaInP using HCl/H_3PO_4. A reactive ion etch process was used to prevent undercut of the GaAs associated with wet chemical etching. The wet etch is highly selective and terminates abruptly at the lower GaAs layer, whose role is to protect the underlying p-doped

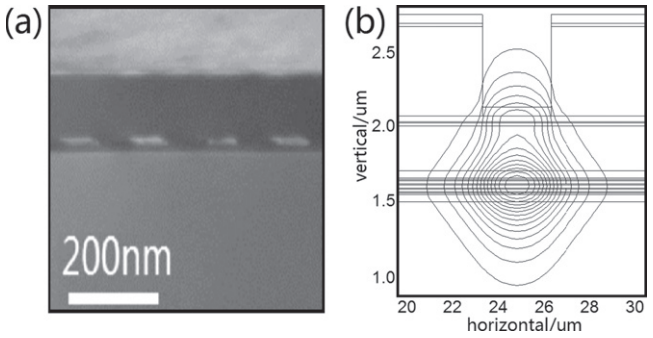

Figure 2. (a) TEM cross-section through the grating (i.e. section taken parallel to the ridge, along the stripe) and (b) Fimmwave simulation of mode profile.

$Al_{0.42}Ga_{0.58}As$ layer from being exposed to atmosphere. This etch is laterally pinned by the previous GaAs dry etch process and can be performed either with or without removal of the patterned PMMA, using the upper GaAs layer as the etch mask. Compared to dry etching the complete grating, it is expected that the wet chemical etch will result in less ion-induced surface damage and the large separation between grating and active is advantageous in minimising damage to the underlying QWs.

Following etching, the PMMA was removed and a simple clean process was performed, including O_2 plasma ash, and a wash in 1% diluted HF. The wafer was then returned to the reactor for overgrowth. 100 nm p-doped GaAs was overgrown to infill and planarize the index-coupled DFB grating, before 600 nm n-doped GaInP (lattice-matched to GaAs) opto-electronic confinement layer, and 20 nm of GaAs completed the overgrowth. Planarization of the gratings is important to ensure high quality GaInP can be grown upon the grating, to prevent corrugation of the waveguide and to simplify grating coupling calculation. In order to infill and planarize the grating, the GaAs layer was grown at a higher temperature than is typically used for GaAs. This imposes a minimum thickness limitation on the GaAs layer in order to adequately planarize the surface prior to GaInP growth. Thinner GaAs layers, such as those used previously [2] and incorporated in our initial design, were defective in planar areas on test overgrowth samples. Although higher quality overgrowth was observed in the grating areas, this would not be suitable for future integrated devices, which would require components to be processed within these planar areas. Overgrowth quality was significantly improved by using a thicker GaAs planarization layer. A dark-field 002 TEM, recorded for a cross-section along the grating, is also shown in figure 2(a), demonstrating high quality infill and planarization of the InGaP grating with subsequent n-doped InGaP growth above, using the modified thickness of GaAs for infill and planarization.

Simulation and design

The SAS–DFB laser was originally designed to incorporate both upper and lower $Al_{0.42}Ga_{0.58}As$ cladding layers. Optical confinement in the grating was designed for $KL = 1$ whilst also maintaining strong optical confinement with the QWs. Fimmwave software was used to simulate the optical profile

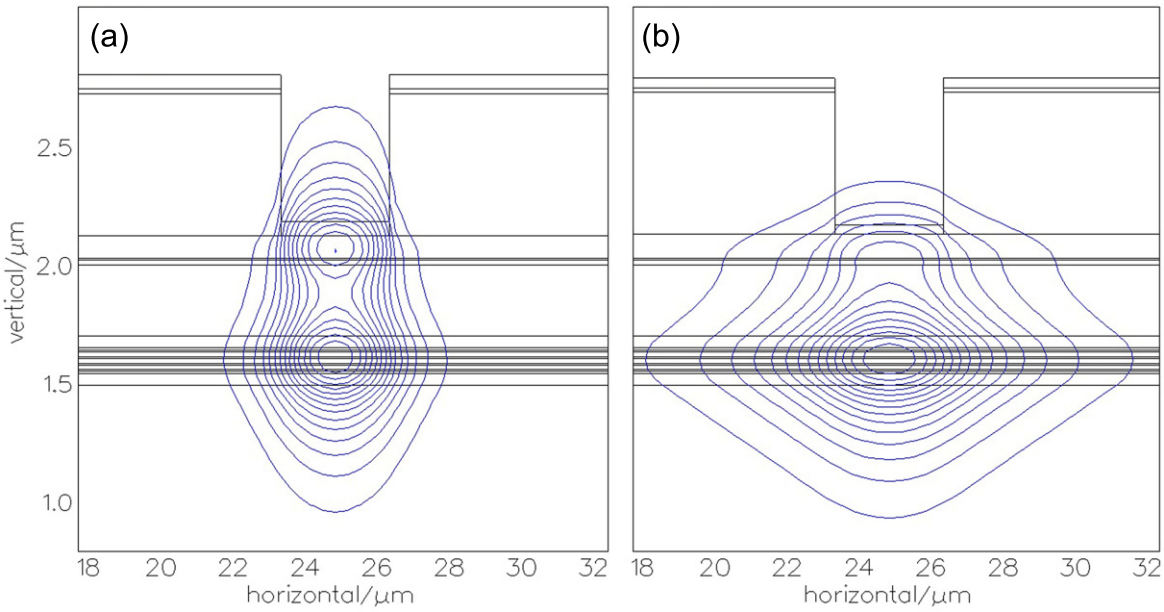

Figure 3. Waveguide simulation (Fimmwave) of increased GaAs from 45 to 100 nm showing: (a) additional guided mode in the thicker GaAs planarization layer and (b) single fundamental mode profile enabled using new parameters.

and calculate overlaps in the structures, using refractive indices at 1000 nm of 3.5 for GaAs, 3.3 for $Al_{0.42}GaAs$, 3.14 for $Al_{0.7}GaAs$, and 3.17 for GaInP. Table 1 outlines the optical confinement and optical far-fields simulated for this design with 45 nm of infill and planarization GaAs grown above the GaInP grating, in column (1).

Essentially, this design is an amalgamation of the GaAs DFB laser in [2] with the GaAs SAS laser structure in [6], placing the grating layers immediately below the n-doped GaInP opto-electronic confinement layer. In order to achieve high quality gratings, the requirement to grow 100 nm GaAs in the first regrowth stage results in an inevitable change in the simulated optical mode profile, which now also resides in an additional guided mode some distance above the active region, as illustrated in figure 3(a), when using the same cladding layer composition. This therefore required a re-design of the layer structure to ensure that appropriate optical confinement can be achieved in both the grating and in the QWs. One strategy could be a re-design of both the upper and lower cladding compositions, and therefore growth of a new planar wafer. Another strategy would be to make use of the tailorability of $Al_xGa_{1-x}As$, which is virtually lattice-matched to GaAs for all compositions, x. We are therefore afforded full flexibility in our choice of Al_x composition for use in the upper cladding layers. Additionally, we may also change the thickness of GaAs that is grown first in the second regrowth step. Therefore, it is entirely feasible that sufficient modification to the optical waveguiding can be achieved by changing only the layers in the subsequent 2nd regrowth step, rather than necessitating growth of a new starting wafer with different lower cladding composition.

The ability to tune the Al_x composition in the overgrown cladding layers is a unique attribute of the GaAs/GaInP SAS design as compared to alternative strategies for buried waveguides, such as Al-free approaches. Full tailoring of the optical mode is possible through optimisation of two main variables in the subsequent second overgrowth stage: the Al_x composition and the GaAs thickness. Figure 4(a) plots the optical confinement factor in both the grating and in the QWs, simulated as a function of Al_x composition with the GaAs thickness fixed at 60 nm (as per our original design). This demonstrates that confinement in the grating can be reduced towards our target value through use of higher composition Al_x in the upper cladding layers. Above $x \sim 0.4$, optical confinement in the QWs is sufficiently high and approximately constant. An Al_x composition of $x = 0.7$ was deemed to be an appropriate upper limit for ease of device fabrication and also taking into account the potential reliability issues associated with higher Al compositions.

Figure 4(b) plots the same simulation as a function of the thickness of GaAs grown in the second regrowth stage but with the composition of Al_x fixed at $x = 0.7$, as decided from

Table 1. Parameters used in the original and modified design together with the expected resultant optical properties.

	(1) Intended 45 nm GaAs planarisation	(2) Now with 100 nm GaAs planarisation
Upper $Al_xGa_{1-x}As$	$x = 0.42$	$x = 0.7$
2nd GaAs in-fill	60 nm	40 nm
$\Gamma_{Grating}$	0.0033	0.0031
Γ_{QWs}	0.0526	0.0531
Far-field FWHM-slow	9.7°	6.9°
Far-field FWHM-fast	43.1°	46.1°

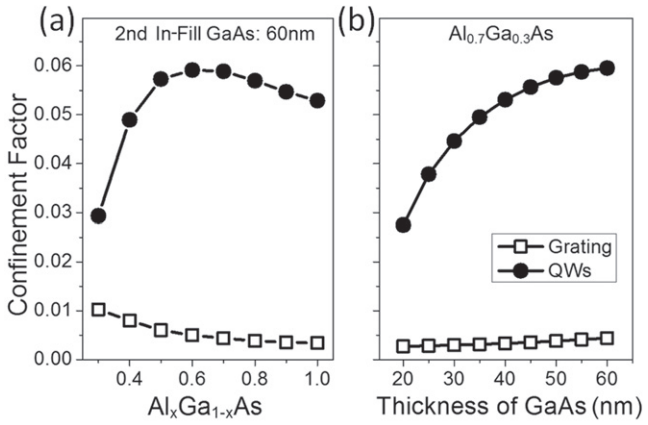

Figure 4. Simulated optical confinement factor in the grating and quantum wells as a function of (a) Al_x composition in $Al_xGa_{1-x}As$ for fixed 2nd regrowth GaAs thickness of 60 nm, (b) thickness of 2nd regrowth GaAs for fixed Al_x composition of $Al_{0.7}Ga_{0.3}As$.

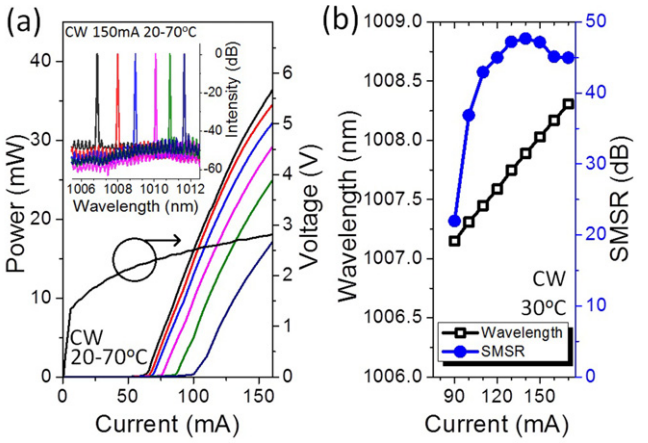

Figure 5. (a) Power versus current characteristic, recorded over a range of substrate temperatures from 20 °C to 70 °C with the inset showing the corresponding lasing peak at 150 mA CW over the range, and (b) the SMSR and wavelength plotted as a function of CW current at 30 °C.

figure 4(a). At 40 nm thick GaAs, our target value of optical confinement factor in the grating is reached whilst also exhibiting a reasonably high optical confinement factor in QWs. With these parameters included in the design, an optical far-field of 46.1°, 6.9° is simulated, as shown in column 2 of table 1. These values are similar to those achievable using our original design (43.1°, 9.7°). The narrower horizontal (slow axis) divergence is a result of a change in the shape of the mode as it interacts with the SAS, but is not expected to present any obvious change in device performance. Therefore, as a direct consequence of the thicker GaAs grating infill and planarization layer, necessary for high quality GaInP growth, the use of thinner GaAs and higher Al composition AlGaAs in the upper cladding layer is viewed as a positive solution to regain the required optical confinements.

Second overgrowth and fabrication

3 μm wide SASs were defined using standard UV optical lithography and transferred to the n-doped GaInP layer by first dry etching through the top GaAs layer using a $SiCl_4$/Ar based ICP process and then wet etching through the GaInP layer, down to the lower GaAs etch stop layer, again using HCl/H_3PO_4. Following photoresist removal and a simple HF clean, a second overgrowth of 40 nm p-doped GaAs, 1500 nm p-doped $Al_{0.7}Ga_{0.3}As$ and a 200 nm GaAs contact layer completed the structure. Following the 2nd regrowth, 600 μm long lasers were processed using standard techniques, aligning a AuZnAu Ohmic contact above the SAS and wet etching isolation trenches through the cladding down to the n-doped GaInP layer to create 100 μm wide electrically isolated devices. TiAu bondpads were deposited above windows etched within a 500 nm thick SiN layer and an InGeAu Ohmic contact was applied to the back of the thinned substrate. Following the application of anti-reflection coatings ($R = 0.1\%$) to one facet only (the other facet remained as-cleaved), devices were mounted epi-side upon Al_2O_3 ceramic tiles for characterisation.

Device characterisation

The performance of a 600 μm long SAS–DFB laser with a 150 nm period grating is demonstrated in figure 5(a) for continuous wave (CW) operation. The laser is kink-free over the temperature range 30°–70°. In practical operation of the DFB laser, a red-shift in the spectral position of the gain peak is unavoidable due to Joule-heating when pumping with high CW current or when operating without adequate heat-sinking provision. In order to ensure that the gain is resonant with the DFB mode when pumped with CW current to achieve relatively high output power, the grating period was designed to be on the long wavelength side of the gain peak in this material to ensure high injected current and high temperature operation. At 20 °C the device reaches lasing threshold at ~65 mA with a kink exhibited in the power versus current (P versus I) characteristic at 110 mA. Examination of the electroluminescence spectrum revealed an expected transition from lasing on multiple Fabry–Perot modes below 110 mA to lasing via the single DFB mode above 110 mA. The current–voltage characteristic is also plotted in figure 5(a), demonstrating a resistance of 5.6 Ω.

At elevated substrate temperatures (30 °C–70 °C) lasing proceeded via the DFB mode from threshold. The device exhibits kink-free single mode operation with more than 30 dB side mode suppression ratio (SMSR) from 1.5× threshold current. Figure 5(b) plots both the SMSR and the lasing wavelength between 90 and 170 mA, extracted from the high-resolution electroluminescence spectrum recorded at 30 °C, using an Advantest Q8384 optical spectrum analyser with 0.01 nm resolution. The laser is observed to operate on a single mode with a SMSR of 36.9 dB at 100 mA (~1.5× threshold) rising up ~45 dB at 130 mA (corresponding to >30 mW output power). The P versus I data in figure 5(a) shows that the threshold current rises from 65 to 100 mA over the temperature range 20 °C–70 °C. The spectrum recorded at 150 mA is shown in the inset to figure 5(a) over the same temperature range. A single mode is exhibited, shifting from

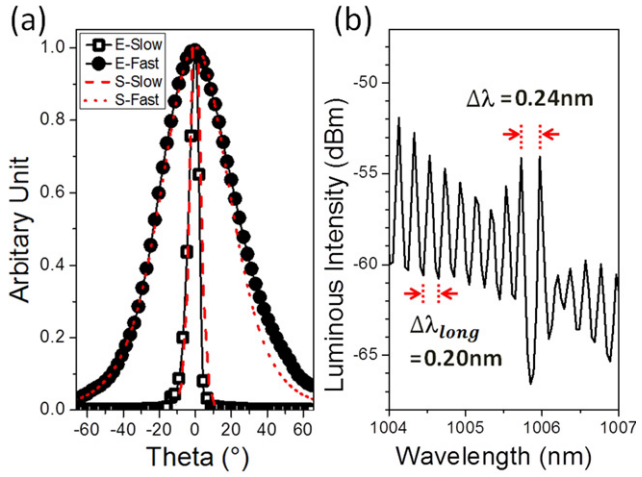

Figure 6. (a) Comparison of simulated (dotted line) and experimental optical far-field for our modified laser. (b) Experimentally measured DBF stop-band with longitudinal mode spacing.

1006.9 nm at 20 °C to 1011.7 nm at 70 °C. This corresponds to a thermal tuning of ~0.1 nm °C^{-1}, maintaining SMSR > 43 dB throughout the temperature range.

Validation of simulation

The optical far-field profiles were measured for our lasers using a standard far-field goniometer with InGaAs detector. The measured horizontal (slow-axis) and vertical (fast-axis) profiles are plotted in figure 6(a). The experimental profiles correlate well with the simulated far-fields, which are shown by the dotted lines superimposed upon the experimental data in figure 6(a). The experimental full-width-at-half-maximum (FWHM) divergence is measured as 49.4° in the fast axis and 6.6° in the slow axis, verifying both the simulation (46.1° and 6.9°) and the origin of emitted light (i.e. via the fundamental lateral mode of the confined SAS). Small differences between the experimental and simulated far-fields are attributed to the effect of gain guiding in the structure and the approximation to a vertical profile of the SAS (i.e.: the shape of the etched stripe) in the simulation, rather than the angled planes provided by the etch process (described in earlier work [6]).

Further correlation between the fabricated device and the simulated optical profile is provided by derivation of the grating coupling coefficient in the SAS–DFB and comparison with the simulated coupling coefficient. By measuring the wavelength spacing ($\Delta\nu$) between two adjacent sub-threshold DFB modes either side of the Bragg wavelength and the longitudinal mode spacing ($\Delta\nu_{\text{long}}$), the coupling coefficient can be deduced from [7]:

$$K_{\text{meas}} = \frac{\pi \times \Delta\nu}{2 \times L \times \Delta\nu_{\text{long}}},$$

where L is the cavity length of device.

Care must be taken for non-zero facet reflectivity since this facet phase relative to the DFB grating distorts the subthreshold emission spectra [8]. However, a good approximation can be

Table 2. Parameters used in the modified design together with the expected resultant optical properties.

Modified design (symmetric)	
$Al_xGa_{1-x}As$	$x = 0.42$
2nd GaAs in-fill	40 nm
1st GaAs in-fill	100 nm
Grating	32 nm
Separation	540 nm
Γ_{Grating}	0.0033
Γ_{QWs}	0.0415

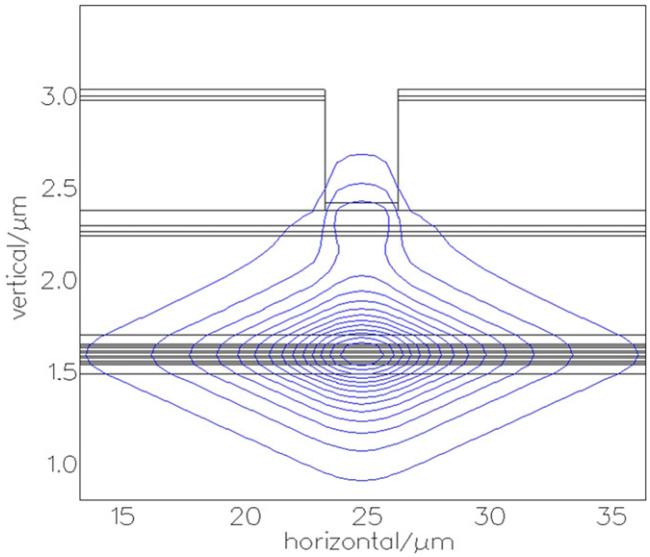

Figure 7. Simulation of mode profile.

derived either by fitting the measured curve for a single laser, or by measuring many devices along the bar (which will have differing facet phase) and selecting the one with the ideal spectrum. The ideal spectrum is one without any residual peaks in the stop band, equal strength peaks either side of the stop band, and these two peaks are stronger than the higher order modes [8]. A range of $\Delta\nu$ was measured across a laser bar. $\Delta\lambda$ between 0.24 and 0.26 nm were measured. With $\Delta\nu_{\text{long}} = 5 \times 10^7$ cm^{-1}, coupling coefficients, K, were calculated between 20.1 and 21.8 cm^{-1}, implying optical confinement factor in the grating, Γ_{grating} between 0.003 and 0.0033, which closely matches that obtained in our simulations (0.0031).

Further simulation for future work

The device reported above was realized through modification to the design of the upper cladding layers due to the emergence of a specific growth requirement for a thicker GaAs layer in the first overgrowth step for planarization. This was enabled through the high level of flexibility offered by our design, and our approach provides a demonstration of this important attribute. However, further simulation has been carried out with the aim of designing a structure appropriate

for use in future integrated designs, with a symmetric composition of Al_x in upper and lower cladding, and lower Al_x composition in the upper cladding. Table 2 shows a modified design with $x = 0.42$. Instead of increasing the Al composition of the upper cladding, this structure is based on a 32 nm thick grating layer and an increased thickness of AlGaAs spacer layer between the grating and the active region of 540 nm. These modifications provide nearly identical confinement factor for the grating and QWs as before, but also with an improved optical mode profile, as shown in figure 7.

Conclusion

We have demonstrated a GaAs-based DFB laser incorporating a first order GaInP/GaAs index-coupled DFB grating built within a SAS buried waveguide structure. Single mode emission was demonstrated at a wavelength of $\sim$1 μm with $>$40 dB SMSR over the temperature range 20 °C–70 °C. We have compared the measured far-field and grating coupling with that simulated for a SAS–DFB incorporating an asymmetric cladding scheme, which demonstrates the flexibility to tailor the optical profile afforded by the SAS approach.

Acknowledgments

The authors gratefully acknowledge a research grant provided by the UK Engineering & Physical Sciences Research Council (EPSRC), reference EP/J004898/1.

References

[1] Muller M, Klopf F, Kamp M, Reithmaier J P and Forchel A 2002 Wide range tunable laterally coupled distributed-feedback lasers based on InGaAs–GaAs quantum dots *IEEE Photonics Technol. Lett.* **14** 1246–8

[2] Stevens B J, Groom K M, Roberts J S, Fry P W, Childs D T D and Hogg R A 2010 Distributed feedback laser employing buried GaAs/InGaP index-coupled grating *Electron. Lett.* **46** 1076–7

[3] Crump P, Brox O, Bugge F, Fricke J, Schultz C, Spreemann M, Sumpf B, Wenzel H and Erbert G 2012 High-power, high-efficiency monolithic edge-emitting GaAs based lasers with narrow spectral widths *Advances in Semiconductor Lasers* (*Semiconductor and Semimetals* vol 86) ed J J Colemann *et al* (Amsterdam: Elsevier) ch 2

[4] Nido M, Komazaki I, Kobayashi K, Endo K, Ueno M, Kamejima T and Suzuki T 1987 AlGaAs/GaAs self-aligned LD's fabricated by the process containing vapor phase etching and subsequent MOVPE regrowth *IEEE J. Quantum. Electron.* **23** 720–4

[5] Yeh N T, Liu W S, Chen S H, Chiu P C and Chyi J I 2002 InAs/GaAs quantum dot lasers with InGaP cladding layer grown by solid-source molecular-beam epitaxy *Appl. Phys. Lett.* **80** 535–7

[6] Groom K M, Stevens B J, Assamoi P J, Roberts J S, Hugues M, Childs D T D, Alexander R R, Hopkinson M, Helmy, Amr S and Hogg R A 2009 Quantum well and dot self-aligned stripe lasers utilizing an InGaP optoelectronic confinement layer *IEEE J. Sel. Top. Quantum Electron.* **15** 819–27

[7] Tu K Y, Tamir T and Lee H 1993 Multiple-scattering theory of wave diffraction by superposed volume gratings *J. Opt. Soc. Am.* A **7** 1421–35

[8] Kjellberg T, Nilsson S, Klinga T, Broberg B and Schatz R 1993 Investigation on the spectral characteristics of DFB lasers with different grating configurations made by electron-beam lithography *J. Lightwave Technol.* **11** 1405–15